Biointerface Research in Applied Chemistry
Open-Access Journal (ISSN: 2069-5837)

Article
Volume 15, Issue 3, 2025, 44
https://doi.org/10.33263/BRIAC153.044

Integrating the Network Pharmacology and Molecular Dynamic Simulation to Reveal Pharmacological Mechanism of *Arcangelisi Flava* (L.) Merr in Treating Inflammation

Yuliana Rut Yabansabra [1], Anike N. Bowaire [2], Arif Setiawansyah [3], Eva Susanty Simaremare [4], Frans Augusthinus Asmuruf [1,*]

[1] Department of Chemistry, Faculty of Mathematics and Natural Sciences, Cenderawasih University, Jayapura 99352, Indonesia; yyabansabra@yahoo.com (Y.R.Y.); asmuruf@yahoo.com (F.A.A.);
[2] Department of Physic, Faculty of Mathematics and Natural Sciences, Cenderawasih University, Jayapura 99352, Indonesia; anike_kala@yahoo.com (A.N.B.);
[3] Center of Natural Product Extract Laboratory, Akademi Farmasi Cendikia Farma Husada, Bandar Lampung 35134, Indonesia; arif12.setiawansyah@gmail.com (A.S.);
[4] Departement of Pharmacy, Faculty of Mathematics and Natural Science, Cenderawasih University, Jayapura 99352, Indonesia; evasmare13@gmail.com (E.S.S.);
* Correspondence: asmuruf@yahoo.com;

Received: 18.01.2025; Accepted: 11.04.2025; Published: 8.06.2025

Abstract: *Arcangelisi flava* (L.) Merr, a medicinal plant traditionally used in Maribu-Sentani-Papua for various ailments, has shown potential in treating inflammation. However, its pharmacological mechanism of action remains unclear. This study aimed to elucidate the mechanism of pain relief compounds in *A. flava* using network pharmacology, molecular docking, molecular dynamics (MD) simulation, drug-likeness prediction, and ADMET profiling. Network pharmacology analysis identified COX-1 and COX-2 as core targets of *A. flava* in inflammation treatment. Among the compounds studied, 1-3-hydroxy-berberine demonstrated the highest potential as a COX-1 and COX-2 inhibitor, with free binding energies of -42.08 and -37.58 kcal/mol, respectively. Drug-likeness prediction based on Lipinski's rule supported its potential as a drug candidate. Pharmacokinetic predictions using pkCSM revealed favorable properties, including high Caco2 permeability (1.073) and human intestinal absorption (97.87%). The compound showed low central nervous system distribution and blood-brain barrier penetration. Metabolic predictions indicated CYP3A4 metabolism and substrate affinity for CYP2C19, CYP2C9, and OCT2. Toxicity assessments suggested that 1-3-Hydroxy-berberine is non-mutagenic, has low acute toxicity, and poses no significant environmental or skin allergy risks. These findings highlight the potential of 1-3-Hydroxy-berberine as a promising COX-1 and COX-2 inhibitor derived from *A. flava*, warranting further investigation for its anti-inflammatory properties.

Keywords: yellow roots; network pharmacology; molecular dynamic; ADMET.

1. Introduction

Arcangelisi flava (L.) Merr, commonly known as yellow roots in Indonesia, is a medicinal plant of significant importance in traditional Papuan medicine. This liana plant, belonging to the Menispermaceae family, is characterized by its extensive growth, reaching up

to 20 meters in length, and is typically found in lowland areas up to 800 meters above sea level [1]. The distinctive yellow wood of *A. flava* has been a staple in traditional remedies for generations. In Papuan communities, particularly in the Maribu-Sentani region, *A. flava* has been utilized for a wide array of medicinal purposes, one of which is pain relief. This traditional use of *A. flava* for pain management has been supported by various scientific reports, encompassing its anti-inflammatory properties in vitro and in vivo [2–4].

A study reported by Akram *et al*. [3] has shown the anti-inflammatory activity of *A. flava* on egg albumin-induced rat paw edema. A similar study was also conducted by Deniyati, demonstrating that the *A. flava* extract (1 – 3% w/v) effectively decreased the rat paw edema. The infused water of *A. flava* was reported to effectively reduce the expression of COX-2, further highlighting its anti-inflammatory potential [4]. The versatility of *A. flava* as an anti-inflammation agent is supported by its rich phytochemical profile. Previous studies have identified several bioactive compounds in the plant, including six types of quaternary alkaloid compounds (thalifedine, dehydrocorydalim, jatrorrhizine, berberine, pcynarrhin, and palmatin) and three types of tertiary alkaloid compounds (hydroxy-berberine, limacine, and homoarmulin). Furthermore, seven furanoditerpene compounds have been isolated from the stem of *A. flava*, including 6-hyrdoxyarcangelisin, 2-dehidroarcangelisinol, tinophylol, 6-hydroxyfibleucin, 6-hydroxyfibraurin, and fibreucin [5]. However, the complete pharmacological mechanisms in which its bioactive compounds regulate the inflammation pathogenesis remain unclear and have not been fully elucidated.

Recent advances in computational methodologies have revolutionized drug research, offering cost-effective and ethical alternatives to extensive animal testing [6]. These methods enable detailed analyses of ligand-receptor interactions, providing insights into the mechanisms by which active compounds from *A. flava* might interact with key targets [7–9]. The present study aims to integrate network pharmacology and molecular dynamic simulation to elucidate the pharmacological mechanism of *A. flava* in treating inflammation. By focusing on the interaction between the plant's active compounds and key inflammatory mediators, we seek to provide a scientific basis for its traditional use as an analgesic and anti-inflammatory agent. This research not only contributes to the validation of traditional knowledge but also paves the way for potential drug discovery based on the bioactive compounds found in *A. flava*.

2. Materials and Methods

2.1. Materials.

This *in silico* computational study was conducted on a dedicated workstation running Ubuntu 20.04 LTS. The system featured an Intel® Core™ i9-12900KF processor (24 CPU at 3.6 GHz), 32 GB RAM, and an NVIDIA RTX 4060 GPU with 16 GB VRAM. Autodock 4.2 was used for molecular docking, while the AMBER package was utilized for molecular dynamics software. Cytoscape 10.0.1 was used for the network pharmacology study, and Biovia Discovery Studi Visualizer was used for protein and ligand preparation and molecular interaction visualization.

2.2. Network pharmacology study.

A comprehensive network pharmacology study was employed based on the method described by Susianti *et al*. [10] with modifications. Target identification was initially undertaken via the SuperPRED database (https://prediction.charite.de) using the compound's

canonical SMILES. All gene targets obtained were standardized in the UniProt database (https://www.uniprot.org) and underwent cross-matching with inflammation-related genes retrieved from the GeneCards database (https://www.genecards.org) using the Venny 2.0 platform (https://bioinfogp.cnb.csic.es/tools/venny/). The genes then underwent protein-protein interaction analysis using the STRING database (https://string-db.org), followed by visualization and topological analysis using Cytoscape 3.10.1. The core targets obtained from topological analysis were used for inflammation-related disease prediction using the DAVID database (https://david.ncifcrf.gov), KEGG enrichment, and gene ontology biological process analysis using ShinyGO 0.80 (http://bioinformatics.sdstate.edu/go/) with a false discovery rate (FDR) threshold was set to 0.05 [11].

2.3. Molecular docking study.

Macromolecules were downloaded from the Protein Data Bank (http://www.rcsb.org.pdb) with PDB ID 4O1Z for COX-1 and 5IKR for COX-2. The natural ligands of COX-1 are the meloxicam and mefenamic acid of COX-2 [12]. The compounds berberine, 1-3-hydroxy-berberine, fibleucin, jatrotthizine, pacybasin, triacontanylcaffeate, p-hydoxybenzaldehiyde, homoaromoline, and limacine were made into two-dimensional structures using Chemsketch software (Figure 1) and stored in *mol format. After that, all compounds were optimized using Orca software with the DFT method of the B3LYP function, based on set 6-31G9d.

The validation of the docking method was carried out by anchoring natural ligands from the COX-1 receptor and COX-2 receptor using AutoDock 4.2 software. The docking calculation was carried out using the Lamarckian Genetic Algorithm (GADock) and Exhaustive Search (ArgusDock) docking methods [13]. The docking method is said to be good if the RMSD (Root Mean Square Deviation) value is between the conformation of the docking pose and crystallography ≤ 2Å [14]. The molecular docking simulation was carried out by anchoring the test ligand compound to the COX receptor using Autodock Tools. The tethering results were evaluated using the Discovery Studio visualizer (DSV) and evaluated.

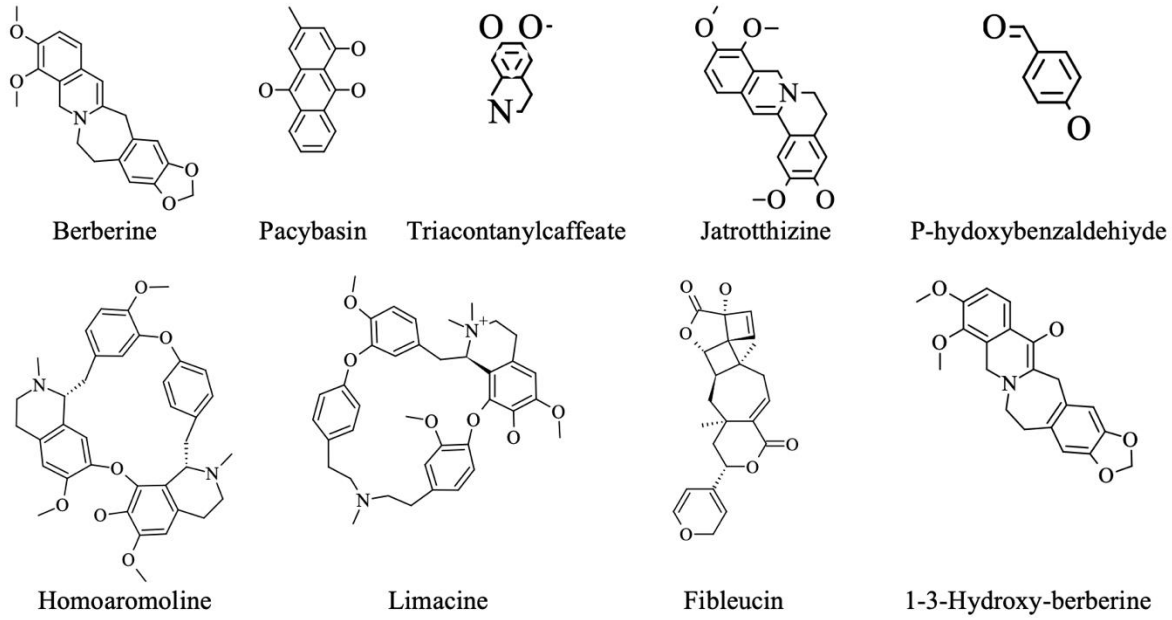

Figure 1. Two-dimensional structure of *A. flava*-derived compounds.

2.4. Molecular dynamic simulation.

Molecular dynamics simulations were conducted using the Amber software package [6,15]. The AMBER ff14SB force field was employed for the protein, while the General Amber Force Field (GAFF) was used for the ligand. The protein-ligand complex was solvated in an octahedral box using the TIP3P water model. Na+ and Cl- ions were added to the solvent to neutralize the system's charge and simulate physiological conditions. The simulation protocol included energy minimization, followed by equilibration under constant volume (NVT) and constant pressure (NPT) conditions. Throughout the simulation, the temperature was maintained at 310K using a Langevin dynamics thermostat, and the pressure was kept at 1 atm. Long-range electrostatic interactions were handled using the Particle Mesh Ewald method. The production MD run was carried out for 200 ns. Analysis of the simulation trajectory included calculations of Root Mean Square Deviation (RMSD), Root Mean Square Fluctuation (RMSF), hydrogen bonding patterns, and MM-GBSA free energy estimates. Visual Molecular Dynamics (VMD) software and Biovia Discovery Studio 2021 were utilized for further analysis and visualization of ligand interactions.

2.5. Drug-likeness and ADMET prediction.

Lipinski's rules and ADMET pharmacokinetics were calculated using web pKCSM (http://biosig.unimelb.edu.au/pkcsm/prediction). Lipinski parameters include P log ≤ 5, molecular weight ≤ 500 g/mol, hydrogen bond donor ≤ 5, and hydrogen bond acceptor ≤ 10 [16].

3. Results and Discussion

The study of *A. flava* represents a significant step towards validating the traditional uses of this plant by the Papuan community, particularly as an anti-inflammatory agent. By employing a multi-faceted approach combining network pharmacology, molecular docking, and molecular dynamic simulation, this research bridges the gap between traditional knowledge and modern scientific understanding. This comprehensive methodology not only addresses the pressing need for scientific validation of traditional remedies but also aligns with the growing global interest in natural products for drug discovery [17]. *A. flava* has been used traditionally for various medicinal purposes, including treating inflammation [18]. However, like many traditional remedies, its use has been based primarily on empirical evidence passed down through generations. The increasing global interest in natural products for drug discovery necessitates rigorous scientific investigation to validate these traditional claims [17]. This study addresses this critical need by employing modern computational and molecular biology techniques to provide a scientific basis for the plant's anti-inflammatory properties.

3.1. Network pharmacology study.

A total of 285 targets were obtained due to the gene mining of all compounds from the SuperPRED database, along with 1066 inflammation-related genes from the GeneCards database. Cross-matching compound-disease genes revealed 138 (11.4%) common genes of *A. flava* and inflammation-related genes. The PPI network construction and topological analysis revealed ten core targets, including HSP90AA1, STAT3, PTGS1, PTGS2, NFKB1, HIF1A, PIK3CA, PPARG, APP, and HSP90AB1. The complete PPI network is depicted in Figure 2.

These core targets illustrated a high degree of connectivity among others, suggesting they might contribute significantly to inflammation pathogenesis [19].

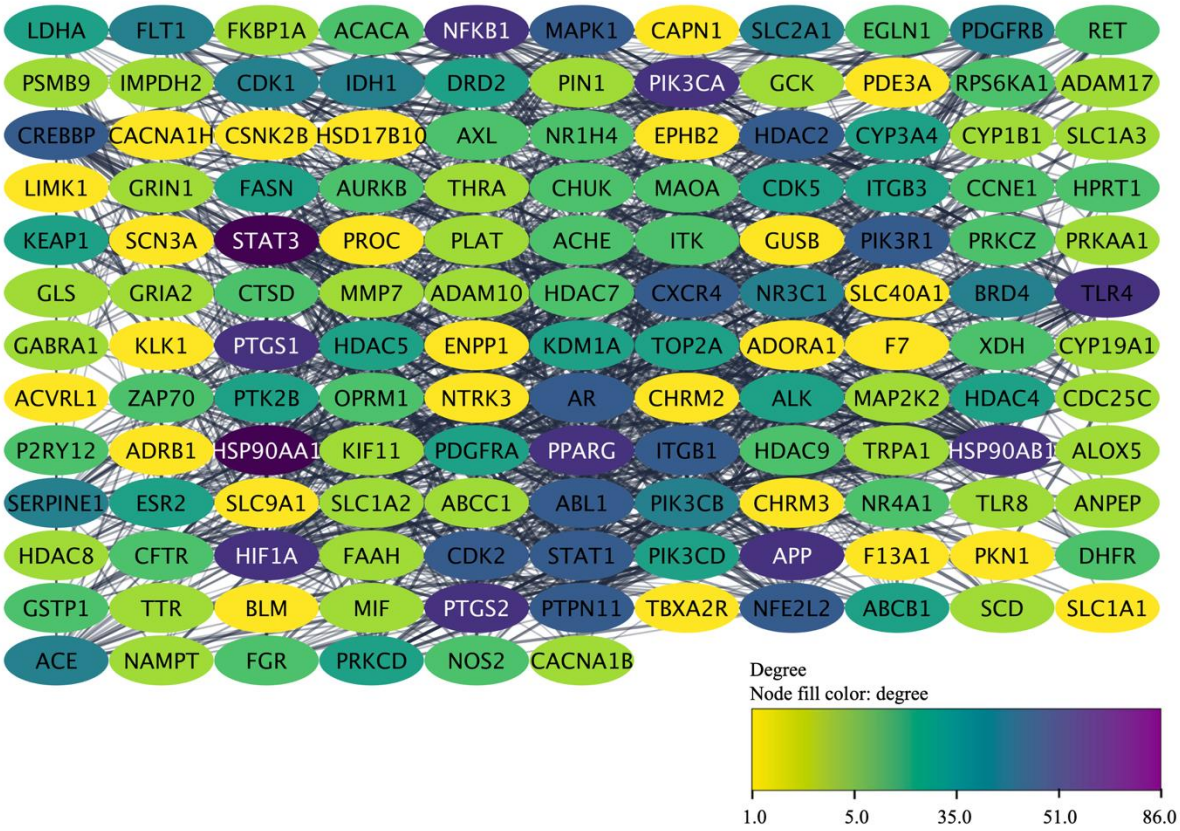

Figure 2. The PPI network illustration. The circular node color shift from yellow to purple represents a high degree of connectivity.

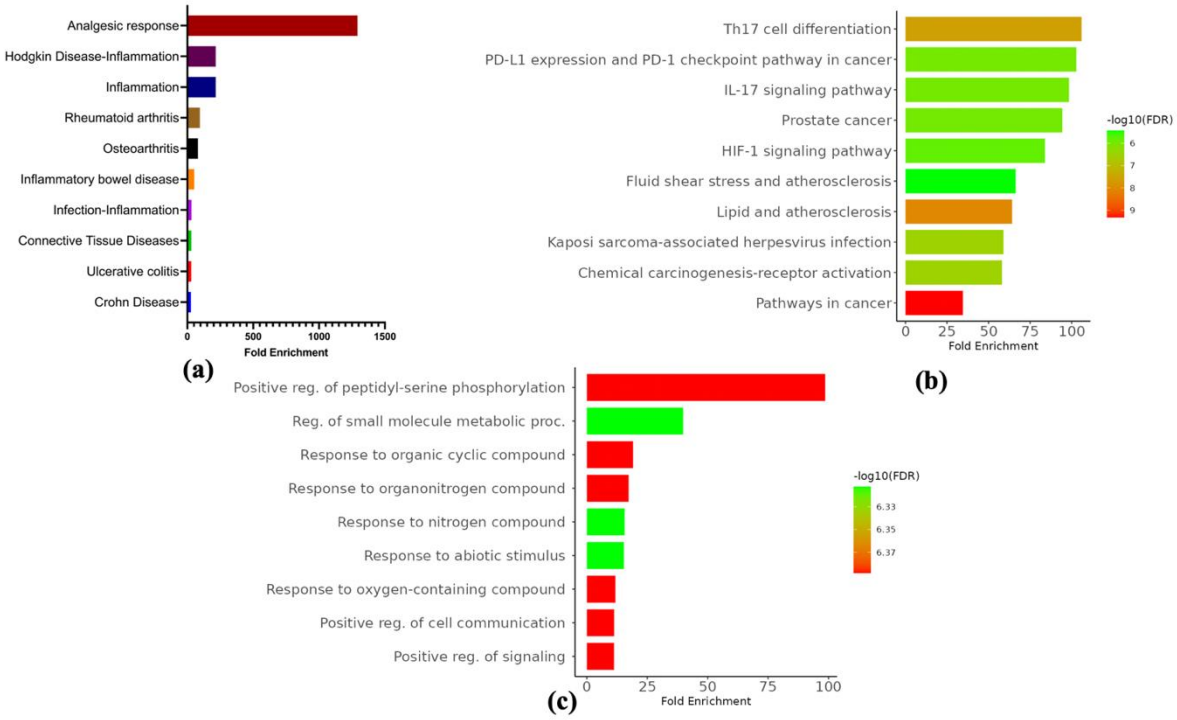

Figure 3. Enrichment analysis result. **(a)** Diseases prediction; **(b)** KEEG pathways; **(c)** GO biological process related to ten core targets.

Enriching the KEGG and GO biological process has provided mechanistic insight into *A. flava* in regulating inflammation pathogenesis (see Figure 3). The Th17 cell differentiation

and IL-17 signaling pathways stand out as the most prominent pathways in how *A. flava* regulates the inflammation process (Figure 3b). The Th17 cell differentiation and IL-17 signaling pathway mechanism implicated in the study were extrapolated and refined based on the canonical pathway map available in the KEGG database (https://www.kegg.jp/pathway/hsa04659 and https://www.kegg.jp/pathway/hsa04657). Further insights into the compound's diverse effects were provided by GO biological process analysis (Figure 3c). The results highlighted the *A. flava*'s role in modulating responses to various stimuli, both external and internal. Specifically, it showed involvement in the regulation of peptidyl-serine phosphorylation and small molecule metabolic processes that have been known to alleviate inflammation.

A comprehensive network diagram was constructed to visually represent the intricate relationships between *A. flava*, its key molecular targets, and the associated medical conditions (refer to Figure 4). This graphical depiction was based on the core targets identified in the study and their linked diseases. In this work, PTGS1 (COX-1) and PTGS2 (COX-2) are found to be the most frequent in inflammation-related diseases, making them the main focus for further analysis.

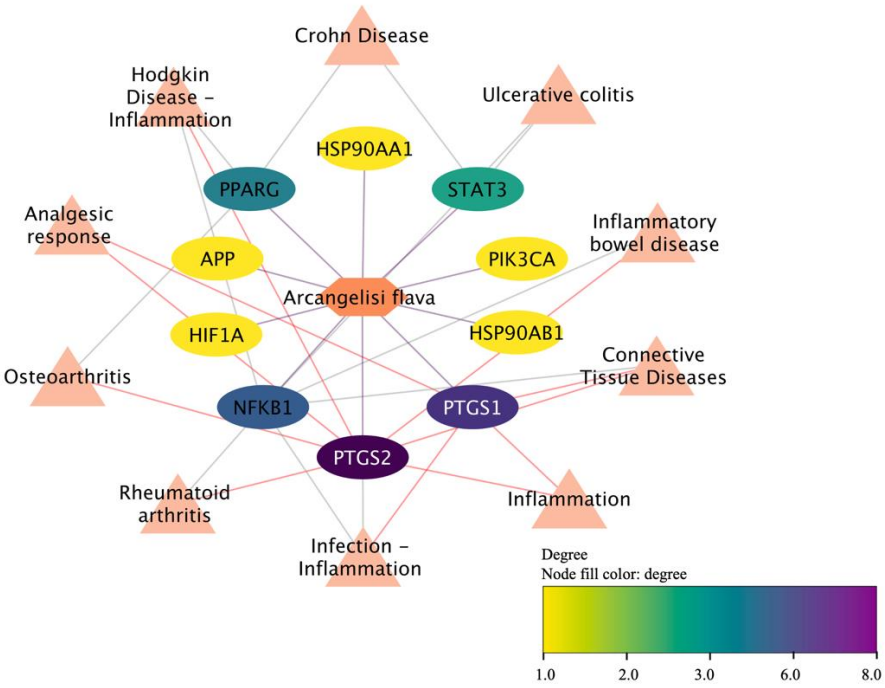

Figure 4. Sample – genes – diseases network. The circular node color shift from yellow to purple represents a high degree of connectivity, with the red lines highlighting the most frequent genes connected with the diseases.

Identifying COX-1 and COX-2 as the most prominent core targets is significant, as these enzymes play crucial roles in the inflammatory process and are well-established targets for anti-inflammatory drugs [20–22]. The involvement of IL-17 signaling pathways and Th17 cell differentiation, as revealed by the KEGG pathway analysis, provides additional insights into the potential immunomodulatory effects of *A. flava*. IL-17 is a pro-inflammatory cytokine associated with various inflammatory disorders, and targeting this pathway could offer a novel mechanism for anti-inflammatory action [23,24]. This finding suggests that *A. flava* might have broader anti-inflammatory effects beyond COX inhibition, potentially modulating adaptive immune responses. Identifying COX-1 and COX-2 as prominent targets of *A. flava* compounds, alongside the involvement of IL-17 signaling pathways and Th17 cell differentiation, presents a complex and interconnected picture of inflammation regulation. Cyclooxygenase enzymes,

particularly COX-2, play a crucial role in producing prostaglandins, which are key mediators of inflammation [25]. Interestingly, recent research has revealed a significant relationship between COX-2-derived prostaglandins and the IL-17/Th17 axis, suggesting a more intricate involvement of COX enzymes in inflammatory processes than previously thought [26–28].

Prostaglandin E2 (PGE2), a primary product of COX-2 activity, has been shown to promote Th17 cell differentiation and IL-17 production [26,29,30]. PGE2 enhances the expression of IL-23 and IL-1β receptors on T cells, which are critical for Th17 differentiation. Moreover, PGE2 can directly act on T cells to induce the production of IL-17 through the EP2 and EP4 receptors [31]. Conversely, IL-17 has been found to induce COX-2 expression in various cell types, creating a positive feedback loop that can perpetuate inflammation [32]. This bidirectional relationship between COX-2 and IL-17 signaling suggests that targeting COX enzymes could have downstream effects on the IL-17/Th17 axis, potentially explaining the broader anti-inflammatory effects observed with some COX inhibitors. In the context of *A. flava*, the dual targeting of COX enzymes and modulation of IL-17 signaling pathways could provide a more comprehensive anti-inflammatory effect than targeting either pathway alone. By inhibiting COX enzymes, *A. flava* compounds may not only reduce prostaglandin production but also indirectly modulate Th17 cell differentiation and IL-17 production.

3.2. Molecular docking and dynamic studies.

The initial process in this work was validating the docking protocol, which exhibited an RSMD value of < 2 Å (summarized in Table 1), suggesting the docking protocol is valid and acceptable to be implemented in assessing the test ligand affinity. The conformation of the re-docking ligands possesses similar poses to the experimental native ligands, as depicted in Figure 5.

Table 1. Grid-box adjustment and coordinate of COX-1 and COX-2.

Parameter	**COX-1**	**COX-2**
Inhibitor	Oxidoreductase/oxidoreductase inhibitor	Oxidoreductase
Center box	34.457	240.111
	39.941	113.022
	81.309	42.929
Grid box	40 x 40 x 40	
Spacing	0.375 Å	

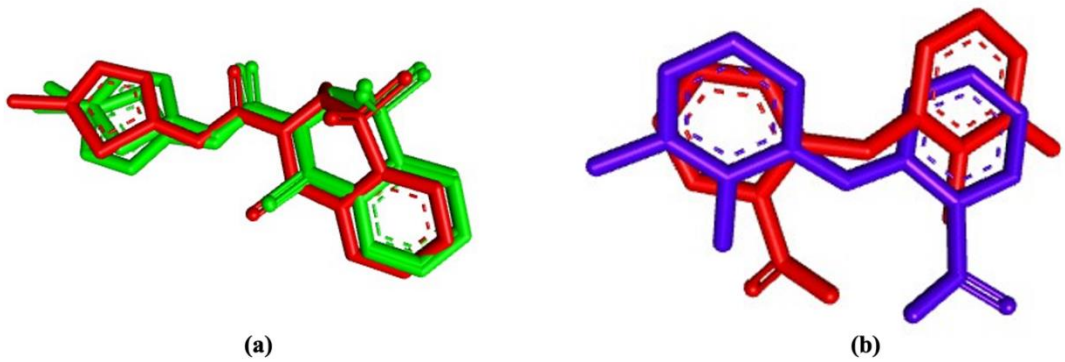

Figure 5. Superimposed of re-docking ligand with original native ligand from **(a)** COX-1; **(b)** COX-2.

Molecular docking of the test ligands has given insight into *A. flava* molecular interaction with COX-1 and COX-2. Table 2 summarizes the binding affinity of *A. flava* compounds with COX-1 and COX-2, illustrating only fibleucin (-10.01 kcal/mol) that exhibited more negative free binding energy than meloxicam (-9.46 kcal/mol). However, its binding energy is only better on the COX-1, while poorer on the COX-2, suggesting fibleucin

is a prominent inhibitor candidate for COX-1. On the other hand, berberine (-8.35 kcal/mol) demonstrates a comparable free binding energy to meloxicam (-8.6 kcal/mol) on COX-2, even better than mefenamic acid (-7.08 kcal/mol), indicating that berberine might act as COX-2 inhibitor. In contrast, two *A. flava* compounds, homoaromoline and limacine, showed positive binding energy values in COX-1 and COX-2, signifying their unstable ligand-macromolecule complexes with COX-1 and COX-2. This unstable complex between ligand and macromolecule often leads to the ligand's propensity to be dissociated from the macromolecule.

Table 2. Results of locular docking of a bioactive compound derived from *A.flava*.

Ligands	COX-1			COX-2		
	BE (kcal/mol)	**kI (uM)**	**Types of AA interactions**	**BE (kcal/mol)**	**kI (uM)**	**Types of AA interactions**
Meloxicam	-9.46	115.93 nM	Hydrogen Bonding (HB) (Ser 530), Sulphuric Bonds (SB) (Trp 387), Pi Alkyl bonding (PAB (Met 522, Leu 384, Ala 527, Val 349, Ile 345, Leu 531)	-8.6	495.89 nM	HB (Ser 530), SB (Phe 381, Phe 205, Trp 387), Amida Pi Stacked (Gly 526), PAB (Ala 527, Leu 352, Val 349, Val 523, Leu 534, Val 228, Phe 209)
Mefenamic acid	-8.11	1.14u M	HB (Ser 530, Tyr 385), pi sigma bonding (Ile 523), PAB (Tyr 355, Phe 518, Leu 352, Ala 527), pi T-shaped bond (Trp 387, Gly 526)	-7.08	6.52 uM	HB (Ser 530), SB (Met 522), PAB (Val 349, Ala 527, Leu 352, Trp 387, Phe 381, Leu 384, Tyr 385, Val 523)
Fibleucin	-10.0	46.85 nM	Unfavorable bond (Val 349), PAB (Phe 518, Leu 352, Ile 523, Ala 527, Val 116, Tyr 355)	-7.6	2.68 uM	HB (Arg 120, Tyr 355, Val 349), PAB (Leu 352, Phe 205, Tyr 385, Ala 527, Val 523)
Jatrotthizin e	-8.33	782.38 nM	HB (Met 522), ICH (Gly 526), PAB (Ile 523, Ala 527, Ser 530, Val 349)	-7.33	4.25 uM	HB (Ala 527, Gly 526, Met 522), I Alkil (Leu 359, Leu 531, Val 349, Leu 352, Val 523)
Berberine	-7.61	2.66 uM	HB (Leu 352), PAB (Ser 353, Ile 523, Ala 527, Leu 359, Leu 531, Val 349)	-8.35	752.41 nM	HB (Arg 120, Gly 526), PAB (Leu 352, Val 523, Ala 527, Leu 531, Val 116, Val 349)
1-3-Hydroxy-berberine	-7.33	4.22 uM	SB (Met 113), PAB (Ser 353), I Alkil (Ala 527, Leu 359, Val 349, Leu 531, Leu 352, Ile 523)	-8.05	1.26 uM	HB (Arg 120, Gly 526, Ser 353), PAB (Leu 352, Ala 527, Leu 531, Val 349, Val 116)
Pacybasin	-6.74	11.40 uM	SB (Met 522), PAB (Leu 352, Ala 527, Ile 523, Val 349, Leu 359, Tyr 355)	-6.64	13.53 uM	HB (Ser 530, Ala 527), SB (with 522), PAB (Val 523, Leu 352, Leu 359, Tyr 355, Val 349, Val 523, Leu 352)
Triacontanylcaffeate	-5.31	128.58 uM	HB (Val 349), PAB (Leu 352) I Alkil (Ile 523)	-5.6	78.42 uM	HB (with 522, Ser 530), PAB (Leu 352)
P-hydoxybenzaldehiyde	-4.9	254.24 uM	HB (with 522, Ser 530), PAB (Gly 526, Leu 352, Trp 387)	-4.46	537.27 rm	HB (Ser 530, with 522), PAB (Gly 526, Ala 527)
Limacine	17.23	-	Unfavorable bond (Tyr 355, Arg 120), HB (Ser 530, Ile 523,), PAB (Leu 352, Ala 527, Leu 359, Ile 345, Val 344, Leu 534, Val 349)	128.98	-	Unfavorable bond (Val 116, Ser 353, Val 523, Phe 518, Met 522, Leu 384, Tyr 385, Ala 527, Gly 526, Leu 352, Val 349, Leu 531), HB (Ser 530), PAB (Tyr 355)
Homoaromoline	67.5	-	Unfavorable bond (Tyr 355, Ile 523, Ser 530, Leu 531, Val 116), PAB (His 90, Val 349, Gly 526, Ala 527, Leu 359)	65.54	-	SB (Met 522), unfavorable bond (Tyr 355, Val 523, Leu 352, Leu 384, Phe 381, Tyr 385, Tyr 348, Val 349), HB (Ser 530), PAB (Leu 531)

The behavior, including the binding pose's stability, flexibility, and reliability, of *A. flava* compound to COX-1 and COX-2 has been observed from the MD simulation in 200 ns. The RMSD values, depicted in Figure 6, on the simulation trajectory, provide insights into the

stability of *A. flava* compounds-macromolecule complexes, which begin to be stable from 100 ns to 200 ns, except 1,3-hydroxyberberine. This compound was unstably bound to COX-1, tending to fluctuate at the beginning of the simulation, and started to detach at 175 ns. Not only 1,3-hydroxyberberine but also mefenamic acid demonstrated an unstable bond during the MD simulation. However, this fluctuation lasts for less than 150 ns and starts to be stable at 150 ns to 200 ns.

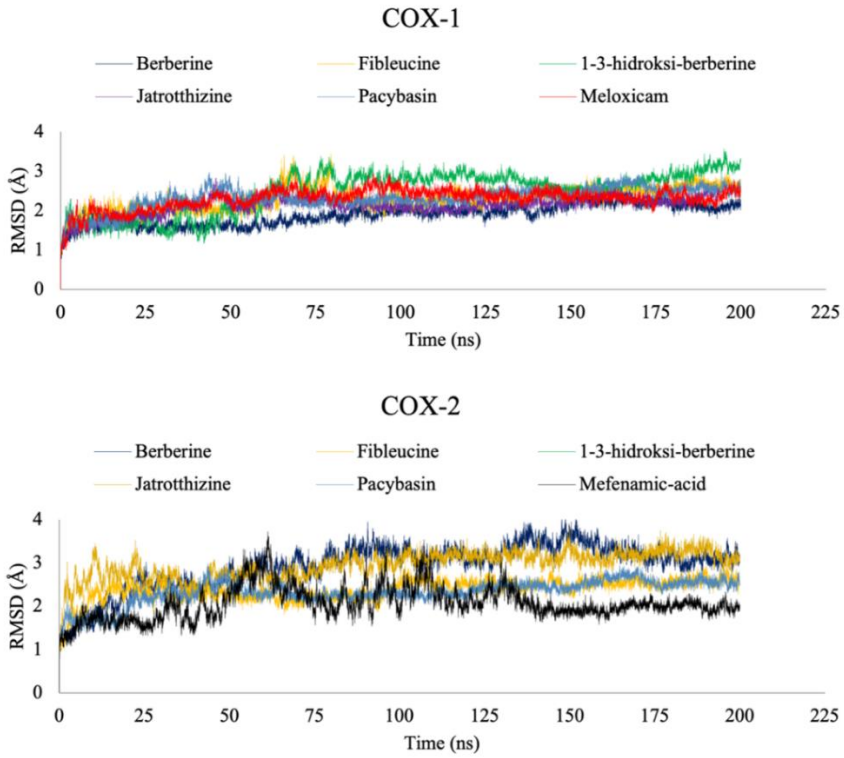

Figure 6. RMSD value from the molecular dynamic of *A. flava* compounds – COX-1/COX-2 complex.

The constant RMSD values illustrate stable interactions occurring between the protein and ligands, suggesting the proteins tend to retain their structural conformations. An analysis of ligand interactions with COX-1 revealed that Val 349, Ala 527, and Leu 531 residues were consistently present in all complex interactions. Conversely, Tyr 385, Trp 385, and Met 522 residues showed no interaction. Four ligands, including berberine, 1,3-hydroxyberberine, jatrotthizine, and pacybasine, exhibited similarities to meloxicam (the native ligand), sharing at least one key residue interaction (as shown in Table 3 and Figure 7). 1,3-hydroxyberberine and berberine demonstrated lower free binding energies (-42.08 kcal/mol and -40.97 kcal/mol, respectively) compared to the native ligand. This suggests superior affinity for these two ligands, as lower free binding energy indicates stronger binding. Additionally, these ligands formed more bonds with receptor residues than the native ligand.

Analysis of ligand interactions with COX-2 revealed that Ala 527 was consistently present in all complex interactions, while Ser 353 showed no interaction. Four ligands, such as berberine, 1,3-hydroxyberberine, jatrotthizine, and pacybasine, demonstrated similarity to the native ligand mefenamic acid, each sharing at least one key residue interaction (Table 3 and Figure 8). 1,3-Hydroxyberberine and berberine exhibited superior binding affinity, with lower free binding energies (-37.58 and -36.94 kcal/mol, respectively) compared to the native ligand. This lower binding free energy indicates stronger interactions. Moreover, these two compounds formed more bonds with receptor residues than the native ligand. According to existing literature, approximately 20 potential residue interactions may occur between ligand enhancers

and COX. Notably, both berberine and hydroxy berberine formed six bonds with COX-1 and seven bonds with COX-2, surpassing the native ligand's interactions.

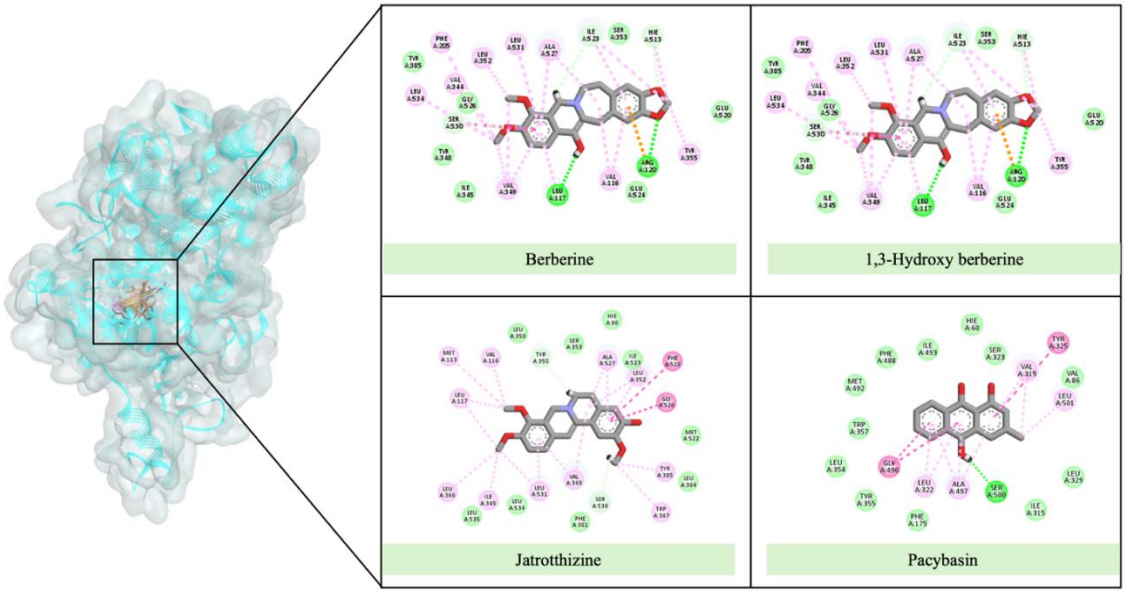

Figure 7. Molecular interaction between several *A. flava* compounds with COX-1 at 200 ns during molecular docking simulation.

Table 3. Data on interaction type, MMPBSA value, and total number of ligand bonds with COX-1 and COX-2.

Ligands	COX-1			COX-2			
	BFE (kcal/mol)	**Types of bond interactions**	**Total of bond interactions**	**BFE (kcal/mol)**	**Types of bond interactions**	**Total of bond interactions**	**Total of bond interactions ligand with COX-1/2**
Meloxicam	-19.78 ± 2.13	Hydrogen bonding (HB) (Ser 530), carbon hyrogen bonding (CHB) (Ser 353, Val 349, Ile 523, Ala 527), pi alkyl bonding (PAB) (Leu 531, Tyr 348, Phe 205)	5	-21.71±0.94	HB (Ser 530, Tyr 348), CHB (Gly 526, Val 523), Sulphur bond (Trp 387), PAB (Ala 527, Val 349, Leu 384, Ala 202)	6	11
Mefenamic acid	-32.63±1.61	HB (Ser 353), PAB (Leu 352, Ala 527, Val 349, Leu 117, Leo 531, Leo 534, Val 344)	5	-30.33±0.35	PAB (Leu 352, Met 522, Leu 384, Tyr 385, Trp 387, Ala 527, Val 349, Val 523)	7	12
1-3-hydroxy-berberine	-42.08±1.19	HB (Leu 117, Arg 120), CHB (Ser 530, Ile 523, Hie 513), PAB (Leu 531, Val 349, Ala 527, Val 116)	7	-37.58±0.26	CHB (Tyr 385, Ser 530, Ala 527, Val 116, Ser 119), Amide pi bond (Gly 526), PAB (Leu 352)	6	13
Berberine	-40.97±0.81	HB (Leu 117, Arg 120), CHB (Ser 530, Ile 523, Hie 513), PAB (Leu 531, Val 349, Ala 527, Val 116)	7	-36.94±0.04	CHB (Leu 384, Ser 530), PPSB (Gly 526, Tyr 355), PAB (Leu 352, Val 349, Ala 527)	6	13
Fibleucin	-34.70±0.35	HB (Asp 362, yr 355), CHB (Phe 361), PAB (Ala 527, Val 349, Leu 531, Leu 117, Leu 366)	4	-28.29±2.73	HB (Tyr 348), CHB (Gly 533, Ala 527, Val 523, Phe 209, Phe 205, Leu 534, Phe 381, Trp 387,	3	7

Ligands	COX-1			COX-2			
	BFE (kcal/mol)	Types of bond interactions	Total of bond interactions	BFE (kcal/mol)	Types of bond interactions	Total of bond interactions	Total of bond interactions ligand with COX-1/2
					Leu 384, Phe 518)		
Jatrotthizine	-27.39±1.99	CHB (Ser 530, Tyr 355), Pi pi stacked bond (PPSB) (Phe 518, Gly 526), PAB (Leu 531, Val 349, Ala 527, Leu 352)	8	-29.02±4.48	PPSB (Tyr 355), PAB (Ala 527, Arg 120, Val 349, Leu 531, Ile 345, Leu 534)	5	13
Pacybasin	-19.68±0.46	HB (Ser 530), ik Pi pi t shaped (Tyr 355), PPSB (Gly 526), PAB (Leu 352, Ala 527, Leu 531, Val 349)	7	-18.40±0.52	HB (Arg 120), Amide pi bond (Gly 526), PAB (Leu 352, Val 349, Ala 527, Leu 359, Leu 117, Leu 531, Met 113, Val 116)	7	14

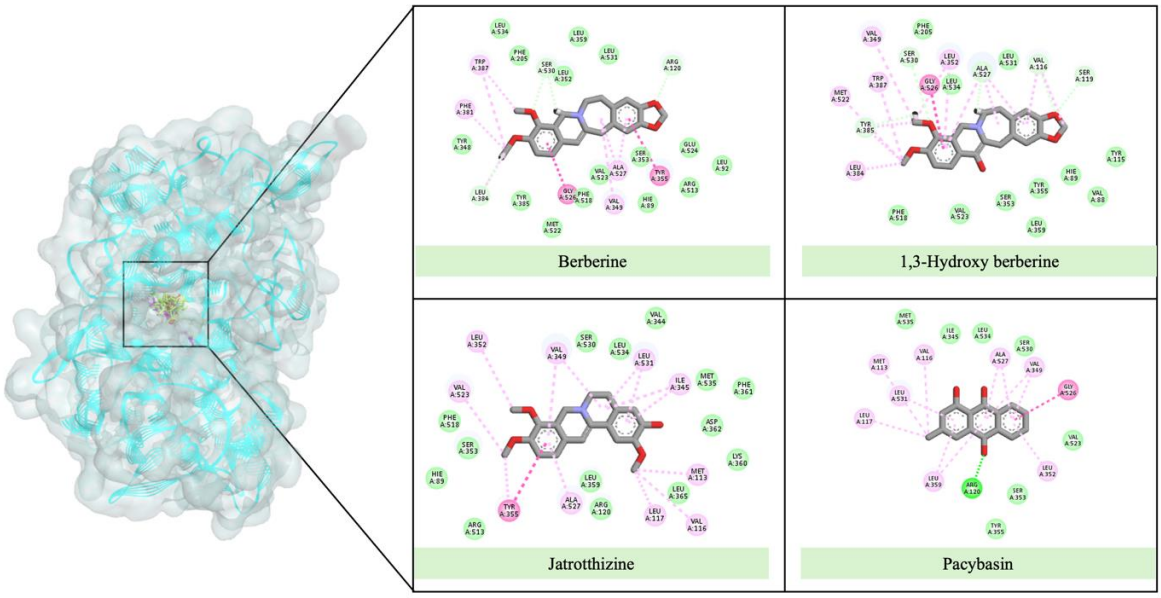

Figure 8. Molecular interaction between several *A. flava* compounds with COX-2 at 200 ns during molecular docking simulation.

The potential ability of *A. flava* to modulate both COX activity and IL-17 signaling could be particularly beneficial in treating chronic inflammatory conditions where both pathways play significant roles. The molecular docking and dynamic simulation studies complement and strengthen the network pharmacology findings by providing a structural basis for the interactions between *A. flava* compounds and their target enzymes. The results demonstrate that several compounds from *A. flava* exhibit stable binding to COX-1 and COX-2 enzymes, interacting with essential amino acid residues in their active sites. Remarkably, these interactions appear to be even more stable than those observed with established NSAIDs such as meloxicam and mefenamic acid. The molecular dynamics simulations reveal that these compounds maintain consistent interactions with key residues in the COX active sites throughout the simulation, indicating a potentially longer-lasting and more effective inhibition. For instance, compounds such as 1,3-hydroxy-berberine and berberine showed lower RMSD values compared to meloxicam and mefenamic acid. These parameters are indicative of a more

stable ligand-protein complex, which could translate to more potent and sustained COX inhibition in vivo [33,34]. Moreover, the binding free energy calculations corroborate these findings, showing more favorable energy profiles for the *A. flava* compounds compared to the reference drugs. This energetic advantage could potentially result in higher binding affinity and, consequently, more effective enzyme inhibition at lower concentrations [35]. Therefore, we can conclude that 1,3-hydroxy-berberine and berberine have greater potential as COX-1 and COX-2 inhibitors. The proposed mechanism of *A. flava* is illustrated in Figure 9.

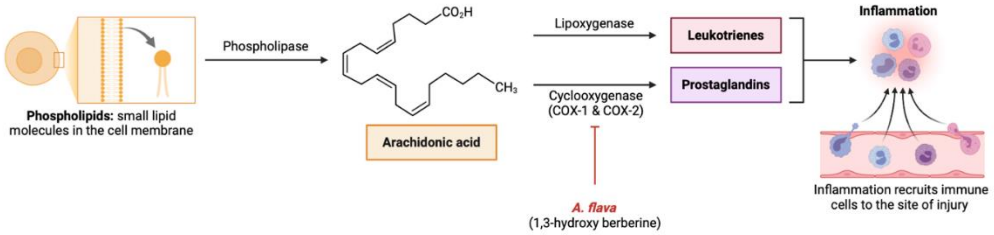

Figure 9. Proposed mechanism of *A. flava* compounds in treating inflammation.

3.3. Molecular docking and dynamic studies.

Lipinski's rule of five (RO5) (i.e., Log P < 5, MW < 500 g/mol, H acceptors ≤ 10, H donors ≤ 5) was used to observe the drug-likeness of *A. flava* compounds. Table 4 provides an intriguing insight into the physicochemical properties of *A. flava* bioactive compounds, illustrating that they me*et al*l the RO5 criteria. This suggests that *A. flava* compounds might share drug-likeness properties similar to oral conventional drugs.

Table 4. Results of drug-like properties analysis based on Lipinski's rule.

Category predictions	MW (≤ 500 g/mol)	LogP (≤ 5)	Rotatable bonds	HB acceptors (≤ 10)	HB donors (≤ 5)	Remarks
Meloxicam	351	1.95092	2	6	2	Meet the criteria
Mefenamic acid	241	4	3	2	2	Meet the criteria
Fibleucin	356.374	2.4528	1	6	11	Meet the criteria
Jatrorrhizine	338.383	3.0818	3	4	1	Meet the criteria
Berberine	336.367	3.0963	2	4	0	Meet the criteria
13-Hydroxyoxyberberine	367.357	2.6761	2	7	1	Meet the criteria
Pachybasin	238.242	2.47602	0	3	1	Meet the criteria

On the oral absorption assessment, *A. flava* generally has good absorption profiles, suggesting it will be well-absorbed when used in the oral route. The Caco2 and HIA values signify this result, which demonstrates all compounds surpassing the threshold of Caco2 (≥ 0.9) and HIA (≥ 80%) minimum requirements, even better than meloxicam, which only provide Caco2 and HIA values of 0.563 and 70.656%, respectively. Even though all compounds exhibit good absorption profiles, some compounds were predicted to be either P-glycoprotein substrate or P-glycoprotein inhibitor, which can alter their absorption profile. Being P-glycoprotein substrate (i.e., jatrorrhizine, berberine, and 13-hydroxyoxy-berberine) will increase the possibility of the compounds being captured by P-glycoprotein when passing through the lipid bilayer and getting flipped to the extracellular matrix [36].

Different from the absorption profile, *A. flava* provides a diverse spectrum of distribution profiles of each compound, as summarized in Table 5. Several compounds, including jatrorrhizine and berberine, demonstrate the highest VDSs (log VDSs > 0.45) among others, highlighting that they will be more distributed in the blood plasm [37]. However, jatrorrhizine's Fu is lower compared to berberine and fibleucin, which exhibit the highest Fu (0.262 and 0.268). This provides significant insight into the number of active portions of

berberine and fibleucin, affecting their pharmacological effect intensities. High Fu often leads to a faster and more intense pharmacological effect, impacted by a high portion of free molecules that can interact with the targets. In contrast, despite the evidence that *A. flava* compounds demonstrated high VDSs and Fu, they are not capable of crossing the blood-brain barrier, as illustrated by their logBB values, which are less than 0.3. However, two compounds (i.e., berberine and pacybasin) demonstrate a logPS value of more than -2, making them considerable to penetrate the CNS.

Table 5. ADMET prediction bioactive compounds derived from *A. flava*

Category predictions		Meloxicam	Mefenamic acid	Fibleucin	Jatrorrhizine	Berberine	13-Hydroxyoxy-berberine	Pachybasin
Absorption	Water solubility (log/mol. L)	-3.464	-3	-3.505	-3.871	-3.973	-3.884	-3.149
	Caco2 permeability >0.90	0.563	1	1.035	1.234	1.734	1.073	1.225
	Intestinal absorption (human)% (>80%)	70.656	96.888	97.68	94.465	97.147	97.87	96.518
	Skin Permeability (log Kp)	-3.031	-3	-3.635	-2.741	-2.576	-2.811	-2.869
	P-glicoprotein substrate	Yes	No	No	Yes	Yes	Yes	No
	P-glycoprotein I inhibitor	No	No	No	No	No	No	No
	P-glycoprotein II inhibitor	No	No	No	Yes	Yes	yes	No
Distribution	VDss (human) (log L/kg)>0.45	-0.133	-1.969	0.198	0.539	0.58	-0.083	0.133
	Fraction unbound (human) (Fu)	0.318	0.053	0.268	0.182	0.262	0.126	0.108
	BBB permeability (Log BB) > 0,3	-0.303	0.321	-0.293	-0.15	0.198	-0.707	0.235
	CNS permeability (Log PS)>-2	-2.443	-2	-3.084	-2.142	-1.543	-2.987	-1.916
Metabolism	CYP2D6 Substrate	No	No	No	No	No	No	No
	CYP3A4 Substrate	No	No	Yes	Yes	Yes	Yes	Yes
	CYP1A2 Inhibitor	No	Yes	No	Yes	Yes	Yes	Yes
	CYP2C19 Inhibitor	No	No	No	No	No	Yes	Yes
	CYP2C9 Inhibitor	No	Yes	No	No	No	Yes	No
	CYP2D6 Inhibitor	No	No	No	Yes	Yes	No	No
	CYP3A4 Inhibitor	No	No	No	No	Yes	Yes	No
Excretion	Total Clearance (log ml/min/kg)	0.07	0.334	0.874	1.222	1.27	0.319	0.109
	Renal OCT2 substrate	No	No	No	No	No	No	No
Toxicity	Ames Toxicity	No	No	No	No	Yes	No	Yes
	Max tolarated dose (log mg/kg/day)	-0.118	0.825	-0.458	0.175	0.144	-0.314	-0.153
	hERG I inhibitor	No	No	No	No	No	No	No
	hERG II inhibitor	No	No	No	Yes	No	No	No
	Oral Rat Acute Toxicity (LD50) (mol/kg)	2.125	2	3.03	2.445	2.571	2.138	2.184

Category predictions	Meloxicam	Mefenamic acid	Fibleucin	Jatrorrhizine	Berberine	13-Hydroxyoxy-berberine	Pachybasin
Oral Rat Chronic Toxicity (LOAEL) (log mg/kg_bw/day)	11.621	2	1.1	1.356	1.89	2.239	2.172
Hepatotoxicity	Yes	No	Yes	Yes	Yes	Yes	No
Skin Sensitisation	No	No	No	No	No	No	No
T.Pyriformis toxi city (log ug/L)	0.473	0	0.299	0.385	0.354	0.361	1.28
Minnow toxicity (Log mM)	1.975	1.142	1.143	0.177	-0.277	1.001	1.3266

In metabolism assessment, various isoforms of CYP450 were used to observe whether *A. flava* compounds can either induce or inhibit the CYP450 enzyme, including CYP2D6, CYP1A2, CYP3A4, CYP2C19, CYP2C9, CYP2D6, and CYP3A4 [38]. Table 5 encompassed the metabolism profile of *A. flava* compounds, demonstrating they are not metabolized by CYP2D6, yet they will be metabolized by CYP3A4. Interestingly, berberine and 13-hydroxyoxy-berberine act as CYP3A4 inhibitors. In another CYP450 isoform, CYP1A2, only fibleucin was observed to be metabolized by this enzyme, while in CYP2C19, only fibleucine will undergo the metabolism process. Furthermore, 13-hydroxyoxy-berberine is predicted to be the inhibitor of both CYP2C19 and CYP2C9, while pacybasin was also found to be the inhibitor of CYP2C9. The complex interplay of *A. flava* compounds provides a comprehensive understanding of their metabolism process. Several compounds demonstrate the potential inhibition effect of some CYP450 isoform, which often leads to increased pharmacokinetic-related drug interaction probability due to the accumulation of drugs or their metabolites [39].

The excretion profile of *A. flava* compounds was assessed by examining their total clearance and potential as renal organic cation transporter 2 (OCT2) substrates, crucial factors affecting drug bioavailability and half-life, influencing dosage and treatment regimens. Table 5 shows all *A. flava* compounds with total clearance exceeding 1 mL/min/kg, categorizing them as high clearance compounds (CLtot > 1 mL/min/kg). This classification is based on a three-tier system: high (>1 mL/min/kg), medium (0.1-1 mL/min/kg), and low (≤0.1 mL/min/kg) clearance [40,41]. Additionally, none of *A. flava* compounds are predicted to act as renal OCT2 substrates. OCT2, a key renal transporter, plays a vital role in the elimination of both endogenous molecules and drugs. The status as an OCT2 substrate is significant, as it increases the potential for drug interactions when administered concurrently with OCT2 inhibitors, an important consideration in drug development and clinical use.

Lastly, the toxicity profile of *A. flava* compounds was evaluated to assess their impact on organismal cells and tissues. This study examined several toxicity parameters, including lethal dose 50 (LD_{50}), mutagenicity (AMES toxicity), and hepatotoxicity. Table 5 shows that *A. flava* compounds have LD_{50} values ranging from 2.138 mol/kg to 3.03 mol/kg. According to Table 4, these compounds have molecular weights (MW) between 238.242 g/mol and 356.374 g/mol. Converting the LD_{50} values from mol/kg BW to g/kg BW yields a range of 520.321 mg/kg BW to 1079.813 mg/kg BW for the *A. flava* compounds in this study. Loomis and Hayes [42] classified compounds with LD_{50} values between 500 mg/kg BW and 5000 mg/kg BW as relatively less toxic. However, despite these high LD_{50} values, some *A. flava* compounds are predicted to have hepatotoxic and mutagenic potential. Specifically, one compound (berberine) is predicted to be both mutagenic and hepatotoxic, while several others (fibleucin, jatrorrhizine, 13-hydroxy-berberin, and pachybasin) are predicted to be either hepatotoxic or mutagenic only.

4. Conclusions

The mechanistic elucidation has observed that *A. flava* contributes to the anti-inflammation by modulating the Th17 cell differentiation and IL-17 signaling pathways along with COX-1 and COX-2 as the core targets. The compound 1-3-hydroxy-berberine has emerged as a promising candidate for COX-1 and COX-2 inhibition, demonstrating impressive binding energies of -42.08 kcal/mol and -37.58 kcal/mol, respectively. Its interactions with these enzymes involve a complex network of bonds, including hydrogen, CHB, pi-alkyl, and amide pi bonding with various amino acid residues. Notably, this compound adheres to Lipinski's rule, suggesting its potential as a viable pharmaceutical agent. Pharmacokinetic predictions paint a favorable picture, with high intestinal absorption and moderate cell permeability, although it shows limited distribution to the central nervous system. Metabolically, 1-3-hydroxy-berberine can be processed by several cytochrome P450 enzymes, excluding CYP1A2, and interacts with the OCT2 transporter. Safety assessments further bolster its drug candidate profile, as it demonstrates non-mutagenicity, low acute toxicity, and minimal risk of skin sensitization or environmental harm. These characteristics collectively position 1-3-hydroxy-berberine as a compelling subject for further investigation in the realm of COX-1 and COX-2 inhibitor development, potentially opening new avenues for therapeutic interventions.

Author Contributions

Conceptualization, F.A.A. and Y.R.Y.; Methodology, Y.R.Y., A.N.B., and A.S.; Software, A.S. and E.S.S.; Validation, Y.R.Y., E.S.S., and A.S.; Formal analysis, E.S.S.; Investigation, A.N.B. and E.S.S.; Resources, F.A.A.; Data curation, A.N.B.; Writing—original draft, Y.R.Y. and E.S.S.; Writing—review & editing, F.A.A. and A.S.; Visualization, A.S.; Supervision, F.A.A.; Project administration, F.A.A.; Funding acquisition, F.A.A. All authors have read and agreed to the published version of the manuscript.

Data Availability Statement

The data presented in this study are available on request from the corresponding author. All datasets used in this research, including protein structures (PDB IDs: 4O1Z and 5IKR), gene targets, and compound structures, were obtained from publicly available databases such as the Protein Data Bank (http://www.rcsb.org), SuperPRED (https://prediction.charite.de), UniProt (https://www.uniprot.org), GeneCards (https://www.genecards.org), STRING (https://string-db.org), and KEGG (https://www.kegg.jp). No proprietary data were generated or used in this study.

Acknowledgments

The authors would like to acknowledge the LPPM Cenderawasih University and The Mahameru National Research and Innovation Agency of the Republic of Indonesia (BRIN)

Conflicts of Interest

The authors declare no conflict of interest.

References

1. Cheng, Q.; Li, F.; Yan, X.; He, J.; Zhang, H.; Wang, C.; He, Y.; Li, Z. Phytochemical and Pharmacological Studies on the Genus Arcangelisia: A Mini Review. *Arabian Journal of Chemistry* **2021**, *14*, 103346, https://doi.org/10.1016/j.arabjc.2021.103346.
2. Deniyati, D. Efek Antiinflamasi Ekstrak Batang Akar Kuning (Arcangelisia Flava (L.) Merr) Terhadap Mencit (Mus Musculus). *Pharmacology and Pharmacy Scientific Journals* **2024**, *3*, 29–34, http://dx.doi.org/10.51577/papsjournals.v3i1.517.
3. Akram, M.M.; Naima, B.; Eddine, M.S.; Soumia, B. Anti-Inflammatory, Anti-Pyretic and Acute Toxicity Effects of n-Butanol Extract of Atractylis Flava Desf in Rats. *Pharmacognosy Journal* **2018**, *10*, 763–767, https://doi.org/10.5530/pj.2018.4.128.
4. Nurrochmad, A.; Mada, G.; Author, C. Anti-Inflammatory Activity Extract of Katola (Arcangelisia Flava (L.) Merr.) on the Expression of Cyclooxygenase-2 Enzyme in Wistar Rats Induced Complete Freund,s Adjuvant (CFA). *International Medical Journal* **2020**, *25*.
5. Pratama, M.R.F.; Suratno, S.; Mulyani, E.V.I. Antibacterial Activity of Akar Kuning (Arcangelisia Flava) Secondary Metabolites: Molecular Docking Approach. *Asian Journal of Pharmaceutical and Clinical Research* **2018**, *11*, 447–451, https://doi.org/10.22159/ajpcr.2018.v11i11.29189.
6. Tiwari, A.; Singh, S. Chapter 13 - Computational approaches in drug designing. In Bioinformatics, Singh, D.B., Pathak, R.K., Eds.; Academic Press: **2022**; pp. 207-217, https://doi.org/10.1016/B978-0-323-89775-4.00010-9.
7. Anatasya Putri, S.; Rani Gustia Maharani, A.; Luthfiana, D.; Chinecherem Nweze, L.; Setiawansyah, A.; Susanti, G. Integrating The Network Pharmacology and Molecular Docking to Uncover The Potential Mechanism Of Rutin In Fighting Diabetes Mellitus. *Ad-Dawaa' Journal of Pharmaceutical Sciences* **2024**, *7*, 39–52, https://doi.org/10.24252/djps.v7i1.49701.
8. Rosa, Y.; Riyanto, R.; Susanti, G.; Setiawansyah, A.; Zuhana, Z.; Fatriansari, A.; Pratama, S.A. Persea Americana Leaf Extract Promotes Wound Healing by Inhibiting NF-KB1. *J Appl Pharm Sci* **2025**, *15*, 160–173, https://doi.org/10.7324/JAPS.2025.218012.
9. Setiawansyah, A.; Susanti, G.; Alrayan, R.; Hadi, I.; Arsul, M.I.; Luthfiana, D.; Wismayani, L.; Hidayati, N. Aaptamine Enhanced Doxorubicin Activity on B-Cell Lymphoma 2 (Bcl-2): A Multi-Structural Molecular Docking Study. *Ad-Dawaa' Journal of Pharmaceutical Science* **2024**, *7*, 1–10, https://doi.org/10.24252/djps.v7i1.46796.
10. Susianti, S.; Bahri, S.; Hadi, S.; Setiawansyah, A.; Rachmadi, L.; Fadilah, I.; Ratna, M.G. Integrating The Network Pharmacology and Molecular Docking Confirmed with In Vitro Toxicity to Reveal Potential Mechanism of Non–Polar Fraction of Cyperus Rotundus Linn as Anti-Cancer Candidate. *Journal of Multidisciplinary Applied Natural Science* **2025**, *5*, 56–73, https://doi.org/10.47352/jmans.2774-3047.228.
11. Xijin Ge, S.; Jung, D.; Yao, R. ShinyGO: A Graphical Gene-Set Enrichment Tool for Animals and Plants. *Bioinformatics* **2020**, *38*, 2628–2629, https://doi.org/10.5281/zenodo.1451847.
12. Orlando, B.J.; Malkowski, M.G. Substrate-Selective Inhibition of Cyclooxygeanse-2 by Fenamic Acid Derivatives Is Dependent on Peroxide Tone. *Journal of Biological Chemistry* **2016**, *291*, 15069–15081, https://doi.org/10.1074/jbc.M116.725713.
13. Amelia, T.; Setiawan, A.N.; Kartasasmita, R.E.; Ohwada, T.; Tjahjono, D.H. Computational Prediction of Resistance Induced Alanine-Mutation in ATP Site of Epidermal Growth Factor Receptor. *Int J Mol Sci* **2022**, *23*, 15828, https://doi.org/10.3390/ijms232415828.
14. Akaho, E.; Fujikawa, C.; Runion, H.I.; hill, C.R.; nakano, H. A Study on Binding Modes of Nonsteroidal Anti-Inflammatory Drugs to COX1 and COX2 as Obtained by Dock4.0. *Journal of Chemical Software* **1999**, *5*, 147–162, https://doi.org/10.2477/jchemsoft.5.147.
15. Singh, S.; Bani Baker, Q.; Singh, D.B. Chapter 18 - Molecular docking and molecular dynamics simulation. In Bioinformatics, Singh, D.B., Pathak, R.K., Eds.; Academic Press: **2022**; pp. 291-304, https://doi.org/10.1016/B978-0-323-89775-4.00014-6.
16. Lipinski, C.A. Lead- and Drug-like Compounds: The Rule-of-Five Revolution. *Drug Discov Today Technol* **2004**, *1*, 337–341, https://doi.org/10.1016/j.ddtec.2004.11.007.
17. Newman, D.J.; Cragg, G.M. Natural Products as Sources of New Drugs over the Nearly Four Decades from 01/1981 to 09/2019. *J Nat Prod* **2020**, *83*, 770–803, https://doi.org/10.1021/acs.jnatprod.9b01285.

18. Pratama, R.R.; Ahsana, D.; Kumar Sahu, R.; Widyowati, R. A Review of Ethnomedicine, Phytochemistry, and Pharmacological Studies on Yellow Roots (Arcangelisia Flava (L.) Merr.). *Malaysian Journal of Chemistry* **2024**, *26*, 224–239.
19. Luthfiana, D.; Utomo, D.H. Network Pharmacology Reveals the Potential of Dolastatin 16 as a Diabetic Wound Healing Agent. *In silico Pharmacol* **2023**, *11*, 23, https://doi.org/10.1007/s40203-023-00161-5.
20. Ju, Z.; Li, M.; Xu, J.; Howell, D.C.; Li, Z.; Chen, F.E. Recent Development on COX-2 Inhibitors as Promising Anti-Inflammatory Agents: The Past 10 Years. *Acta Pharm Sin B* **2022**, *12*, 2790–2807, https://doi.org/10.1016/j.apsb.2022.01.002.
21. Pairet, M.; Van Ryn, J.; Mauz, A.; Schierok, H.; Diederen, W.; Türck, D.; Engelhardt, G. Differential inhibition of COX-1 and COX-2 by NSAIDs: a summary of results obtained using various test systems. In Selective COX-2 Inhibitors: Pharmacology, Clinical Effects and Therapeutic Potential, Vane, J., Botting, J., Eds.; Springer Netherlands: Dordrecht, **1998**; pp. 27-46, https://doi.org/10.1007/978-94-011-4872-6_3.
22. Khan, A.A.; Iadarola, M.; Yang, H.-Y.T.; Dionne, R.A. Expression of COX-1 and COX-2 in a Clinical Model of Acute Inflammation. *J Pain* **2007**, *8*, 349–354, https://doi.org/10.1016/j.jpain.2006.10.004.
23. Suyama, K.; Sakai, D.; Watanabe, M. The Role of IL-17-Mediated Inflammatory Processes in the Pathogenesis of Intervertebral Disc Degeneration and Herniation: A Comprehensive Review. *Front Cell Dev Biol* **2022**, *10*, 857164, https://doi.org/10.3389/fcell.2022.857164.
24. Sun, L.; Wang, L.; Moore, B.B.; Zhang, S.; Xiao, P.; Decker, A.M.; Wang, H.-L. IL-17: Balancing Protective Immunity and Pathogenesis. *J Immunol Res* **2023**, *2023*, 3360310, https://doi.org/10.1155/2023/3360310.
25. Nørregaard, R.; Kwon, T.H.; Frøkiær, J. Physiology and Pathophysiology of Cyclooxygenase-2 and Prostaglandin E2 in the Kidney. *Kidney Res Clin Pract* **2015**, *34*, 194–200, https://doi.org/10.1016/j.krcp.2015.10.004.
26. Lemos, H.P.; Grespan, R.; Vieira, S.M.; Cunha, T.M.; Verri Jr, W.A.; Fernandes, K.S.; Souto, F.O.; McInnes, I.B.; Ferreira, S.H.; Liew, F.Y. Prostaglandin mediates IL-23/IL-17-induced neutrophil migration in inflammation by inhibiting IL-12 and IFNγ production. *Proceedings of the National Academy of Sciences* **2009**, *106*, 5954-5959, https://doi.org/10.1073/pnas.0812782106.
27. Polese, B.; Thurairajah, B.; Zhang, H.; Soo, C.L.; McMahon, C.A.; Fontes, G.; Hussain, S.N.A.; Abadie, V.; King, I.L. Prostaglandin E2 Amplifies IL-17 Production by Γδ T Cells during Barrier Inflammation. *Cell Rep* **2021**, *36*, 109456, https://doi.org/10.1016/j.celrep.2021.109456.
28. Li, H.; Bradbury, J.A.; Dackor, R.T.; Edin, M.L.; Graves, J.P.; DeGraff, L.M.; Wang, P.M.; Bortner, C.D.; Maruoka, S.; Lih, F.B. Cyclooxygenase-2 regulates Th17 cell differentiation during allergic lung inflammation. *American journal of respiratory and critical care medicine* **2011**, *184*, 37-49, https://doi.org/10.1164/rccm.201010-1637OC.
29. Boniface, K.; Bak-Jensen, K.S.; Li, Y.; Blumenschein, W.M.; McGeachy, M.J.; McClanahan, T.K.; McKenzie, B.S.; Kastelein, R.A.; Cua, D.J.; De Malefyt, R.W. Prostaglandin E2 Regulates Th17 Cell Differentiation and Function through Cyclic AMP and EP2/EP4 Receptor Signaling. *Journal of Experimental Medicine* **2009**, *206*, 535–548, https://doi.org/10.1084/jem.20082293.
30. Zhang, W.; Yin, J.; Deng, Y.; Gong, Y.; Sun, X.; Chen, J. Prostaglandin E2 Promotes Th17 Differentiation Induces Corneal Epithelial Cell Apoptosis and Participates in the Progression of Dry Eye. *Arch Biochem Biophys* **2024**, *751*, 109823, https://doi.org/10.1016/j.abb.2023.109823.
31. Chizzolini, C.; Chicheportiche, R.; Alvarez, M.; de Rham, C.; Roux-Lombard, P.; Ferrari-Lacraz, S.; Dayer, J.-M. Prostaglandin E2 Synergistically with Interleukin-23 Favors Human Th17 Expansion. *Blood* **2008**, *112*, 3696–3703, https://doi.org/10.1182/blood-2008-05-155408.
32. Chabaud, M.; Fossiez, F.; Taupin, J.-L.; Miossec, P. Enhancing Effect of IL-17 on IL-1-Induced IL-6 and Leukemia Inhibitory Factor Production by Rheumatoid Arthritis Synoviocytes and Its Regulation by Th2 Cytokines 1. *J. Immunol.* **1998**, *161*, 409-414.
33. Durrant, J.D.; McCammon, J.A. Molecular Dynamics Simulations and Drug Discovery. *BMC Biol* **2011**, *9*, 71, https://doi.org/10.1186/1741-7007-9-71.
34. AlRawashdeh, S.; Barakat, K.H. Applications of Molecular Dynamics Simulations in Drug Discovery. In Computational Drug Discovery and Design, Gore, M., Jagtap, U.B., Eds.; Springer US: New York, NY, **2024**; Volume 2714, pp. 127-141, https://doi.org/10.1007/978-1-0716-3441-7_7.
35. Ganesan, A.; Coote, M.L.; Barakat, K. Molecular Dynamics-Driven Drug Discovery: Leaping Forward with Confidence. *Drug Discov Today* **2017**, *22*, 249–269, https://doi.org/10.1016/j.drudis.2016.11.001.

36. Tandon, V.R.; Kapoor, B.; Bano, G.; Gupta, S.; Gillani, Z.; Gupta, S.; Kour, D. P-Glycoprotein: Pharmacological Relevance. *Indian J Pharmacol* **2006**, *38*, 13-24, https://doi.org/10.4103/0253-7613.19847.
37. Pires, D.E.; Blundell, T.L.; Ascher, D.B. PkCSM . Predicting Small-Molecule Pharmacokinetic Properties Using Graph-Based Signatures. *Journal of Medicinal Chemistry* **2015**, *58*, 4066-4072, https://doi.org/10.1021/acs.jmedchem.5b00104.
38. Amin, M.L. P-Glycoprotein Inhibition for Optimal Drug Delivery. *Drug Target Insights* **2013**, *2013*, 27–34, https://doi.org/10.4137/DTI.S12519.
39. Durán-Iturbide, N.A.; Díaz-Eufracio, B.I.; Medina-Franco, J.L. *In silico* ADME/Tox Profiling of Natural Products: A Focus on BIOFACQUIM. *ACS Omega* **2020**, *5*, 16076–16084, https://doi.org/10.1021/acsomega.0c01581.
40. Paine, S.W.; Ménochet, K.; Denton, R.; McGinnity, D.F.; Riley, R.J. Prediction of Human Renal Clearance from Preclinical Species for a Diverse Set of Drugs That Exhibit Both Active Secretion and Net Reabsorption. *Drug Metab Dispos* **2011**, *39*, 1008–1013, https://doi.org/10.1124/dmd.110.037267.
41. Paine, S.W.; Barton, P.; Bird, J.; Denton, R.; Menochet, K.; Smith, A.; Tomkinson, N.P.; Chohan, K.K. A Rapid Computational Filter for Predicting the Rate of Human Renal Clearance. *J Mol Graph Model* **2010**, *29*, 529–537, https://doi.org/10.1016/j.jmgm.2010.10.003.
42. Loomis, T.A.; Hayes, A.W. CHAPTER 12 - Principles of Biological Tests for Toxicity. In Loomis's Essentials of Toxicology, 4th Edition, Loomis, T.A., Hayes, A.W., Eds.; Academic Press: San Diego, **1996**; pp. 167-204, https://doi.org/10.1016/B978-012455625-6/50012-X.

Publisher's Note & Disclaimer